行政院國家科學委員會專題研究計畫　期中進度報告

原子力顯微鏡研究奈米磊晶技術與製造周期排列之奈米結構(2/3)

計畫類別：個別型計畫
計畫編號：NSC93-2112-M-009-038-
執行期間：93 年 08 月 01 日至 94 年 07 月 31 日
執行單位：國立交通大學電子物理學系(所)

計畫主持人：簡紋濱

計畫參與人員：王敬平，江森正，黃順誠，王雨瑞，魏銘延，歐逸青，葉佳唯

報告類型：精簡報告

處理方式：本計畫可公開查詢

中　華　民　國 94 年 5 月 31 日

中文摘要

本計畫執行分別在(一)奈米顆粒磁性研究，(二)奈米顆粒薄膜成長，(三)使用掃描探針顯微鏡製造奈米結構，(四)奈米線電性研究，(五)自製掃描穿隧電流顯微鏡與小訊號測量儀器等方面各有進展。在奈米顆粒磁性研究方面，我們已能區分軌道順磁與軌道逆磁兩種效應，並發現軌道逆磁現象符合二維量子點的小尺寸修正下之 Landau 逆磁現象。在奈米顆粒薄膜成長方面，我們在室溫 20^{o}C 到 130^{o}C 下都能長出單層膜，並發現高溫成長下可製造極平整圓滑弧型島嶼，與超高真空下原子成長薄膜之機制相同。在製造週期排列奈米結構方面，我們使用金探針在石墨表面上製造出石墨坑洞與金小山丘，改變脈衝電壓之振福與時間，我們可製造出約 10 nm 直徑，高度 1-2 nm 之週期排列的金奈米結構。在奈米線電性研究方面，我們用兩點接線與四點接線方式，發現奈米線與電極間之奈米接點的電性，藉由控制奈米接點的絕緣層厚度,我們可以由下而上製造出取代半導體 pn 結與 JFET 或 MOSFET 電晶體之奈米線電子元件。在自製儀器方面，我們完成室溫掃描穿隧電流顯微鏡的機械設計加工與電子控制器，又完成小訊號測量之小於 1 nA 電流供應器。

關鍵詞：奈米結構成長，奈米結構電性，奈米結構磁性，先進儀器開發

Abstract

We have conducted several ways to approach the goal of our project. Firstly, we have studied orbital susceptibilities of PbSe quantum dots. Two types of orbital susceptibilities, including Curie susceptibility and finite-size corrections to the Landau susceptibility, have been observed. The two effects can easily be separated. We have reported the field, temperature, and size dependence of the two orbital susceptibilities. Secondly, we have prepared thin films of PbSe quantum dots. The quantum dots, like atoms in ultra high vacuum, were deposited on graphite or mica in air. Coverage and temperature dependences of growth have been scanned by using atomic force microscope. Thirdly, we have fabricated periodically arranged nanostructures on graphite surface. Either graphite pits or gold mounds on graphite were formed by using voltage pulse between the tip and the sample. By controlling the amplitude and duration of pulse, we have made periodically spaced gold mounds with a diameter of ~10 nm and a eight of 1-2 nm on the surface. Fourthly, we have studied nanocontact junctions between electrodes and ZnO nanowires by using the e-beam lithography. Two types of nanocontact junctions with different current-voltage characteristics have been found. We demoed bottom-up fabricated nanowire-devices which can be used for replacing pn junctions, and JFET or MOSFET transistors in the near future. Finally, we have home-made an STM with mechanical parts and electronic controllers. We also built a nano ampere current supplier with a noise level as low as 1 %.

Keywords: growth of nanostructures, electrical properties of nanostructures, magnetic properties of nanostructures

(1)奈米顆粒磁性研究

我們製造不同尺寸大小的 PbSe 奈米顆粒，即三維量子點來研究量子點內自由電子做軌道運動所產生的軌道磁化率。量子點的磁化率可區分為居禮順磁與小尺寸修正下 Landau 逆磁，居禮順磁現象可在磁化率隨溫度變化曲線中，低於 10 K 的溫度下觀察到。在高溫下觀察磁化率隨磁場變化顯示小尺寸修正下 Landau 逆磁，並觀察到 zero-field paramagnetic peak。量子點內這兩種軌道磁化率都跟尺寸線性相關，此實驗結果符合理論計算所得二維量子點內小尺寸修正下 Landau 逆磁。

先量測樣品中 PbSe 材料佔 90%重量百分比，其餘 10%為保護量子點的有機分子，包括 TOP 與 oleic acid，我們先移除磁性數據中有機分子的貢獻，其次將磁性結果區分原子順磁，原子逆磁，量子點順磁，與量子點逆磁四個部分。PbSe 原子順磁為零，原子逆磁為-1x10^{-4} emu / mol Oe，將實驗數據中與溫度磁場無關的原子逆磁數據移除，最後的結果如圖 1-1 為量子點的磁性數據。我們在圖中觀察到 10 k 以下有居禮順磁現象，受溫度擾動，在溫度略高區域即迅速減小消失，然而在高溫區域小磁場下，仍然可以觀察到一個順磁現象顯示大於零的磁化率，此為小尺寸修正下 Landau 逆磁。如圖 1-2 所示，o 形與 x 形點分別代表 6.7 奈米與 10 奈米大小的量子點，在 200 K 下所測量到的磁化率隨磁場變化曲線，在低磁場 2000 Oe 以下可觀察到 zero-field paramagnetic peak，符合理論計算之結果，且低磁場所觀察到的順磁，亦對應到圖 1-1 高溫下所觀察到的順磁行為，驗證溫度高於 10 K 的磁性行為皆來自於小尺寸修正下 Landau 逆磁的貢獻。

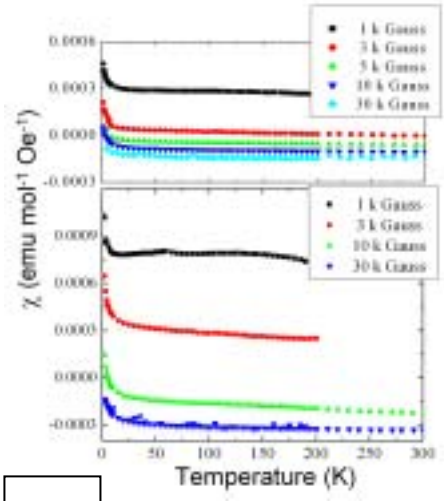

1-1

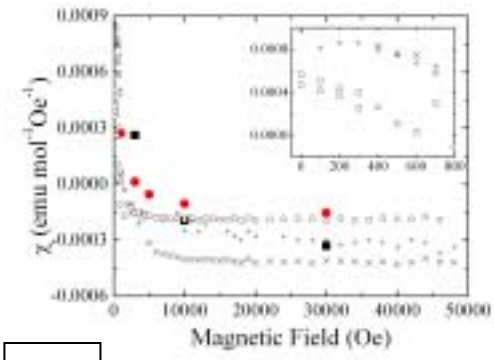

1-2

仔細研究小尺寸修正下 Landau 逆磁，我們觀察到如圖 1-3 的磁滯現象，鐵磁性材料由於原子內 d 軌道電子未填滿造成磁矩，磁矩間有鐵磁或反鐵磁 exchange interaction，形成磁區，磁區受磁場翻轉而產生磁滯曲線。此量子點樣品，並無原子順磁，高溫下也沒有量子點的居禮順磁，竟然觀察到磁滯現象，此結果將讓我們重新解釋奈米磁性。

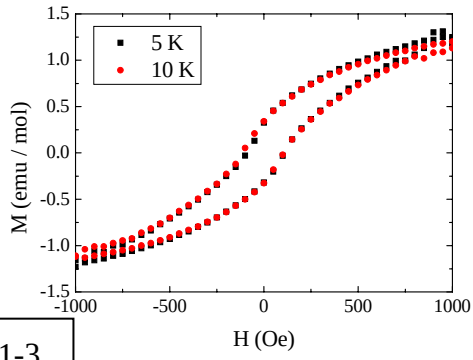

1-3

(2)奈米顆粒薄膜成長

我們將 PbSe 奈米粒子溶在甲苯溶劑中，在不同溫度下滴在石墨或雲母片基板上，待溶劑揮發後使用原子力顯微鏡，觀察奈米粒子成長的機制。在高溫下，我們可以製造出單層 10 奈米高度的薄膜，並且可以取得奈米粒子週期排列的粒子解析度。隨著成長的溫度由室溫 20 ^{o}C 上升到 130 ^{o}C，我們觀察到薄膜的幾何形狀，由樹枝狀改變為圓形島嶼形狀，此成長行為與超高真空下所觀察到原子磊晶之薄膜成長機制相同。

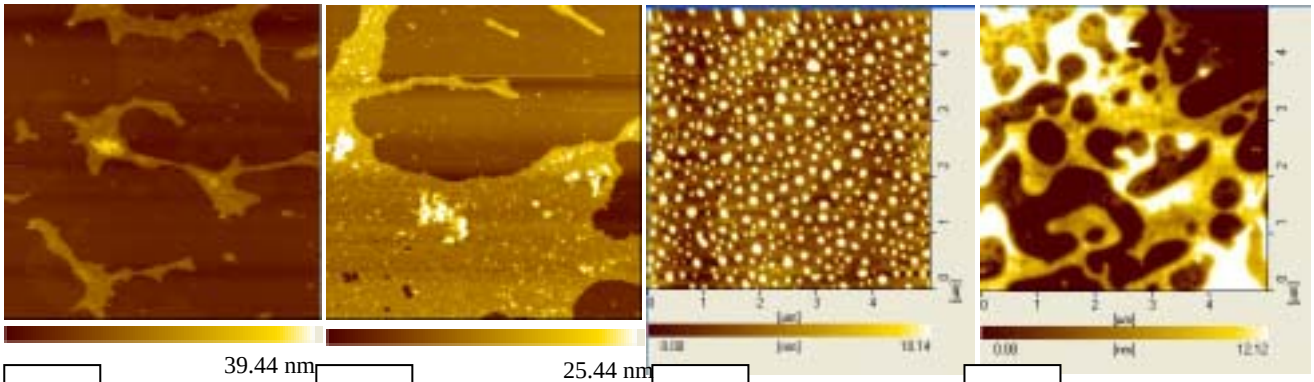

2-1　2-2　2-3　2-4

我們使用加熱板與燈泡直射兩種方式加熱與準備樣品，並使用熱電偶校正溫度，發現燈泡加熱方式有助於移除奈米粒子表面的有機分子保護層。比較石墨、雲母片，與矽等三種基板，發現奈米粒子在石墨基板上成長，最容易長成規則排列平整的單層膜，而控制成長溫度與濃度亦可在雲母片與矽基板上製作平整之奈米粒子島嶼。圖 2-1~2-4 皆為 5 μm x 5 μm 尺寸大小的原子力顯微鏡表面地形圖，基座皆為原子級平整表面，圖 2-1 與 2-2 為室溫 20 ^{o}C 所準備的不同奈米粒子數量(coverage)之成長情形，在室溫下成長能形成 10 奈米厚度的奈米粒子單層膜，初形成之島嶼為樹枝狀，所形成薄膜表面粗糙度較大。在 130 ^{o}C 高溫下成長，隨 coverage 不同形成之島嶼與單層膜如圖 2-3 與 2-4 所示，其初形成為圓弧形島嶼，隨著量增加，可形成平整的奈米粒子單層膜，藉著控制溫度與濃度，我們能掌握奈米粒子的成長與研究其成長機制。

右圖為 700 nm x 700 nm 尺寸大小的粒子影像圖，顯示高溫成長條件下，奈米粒子形成週期排列平整的單層膜，樣品成長溫度為 100 ^{o}C，低於圖 2-3 與 2-4 之成長溫度，所形成的島嶼介於樹枝狀與圓弧形之間。

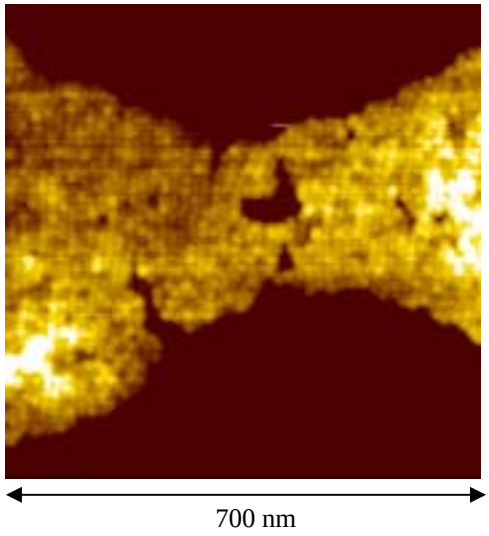

(3)使用掃描探針顯微鏡製造奈米結構

使用鹽酸電化學蝕刻方式製造金針，使用導電式原子力顯微鏡，在探針與石墨基板間製造 0.1-10 豪秒時間長度，3-5 伏特振幅之脈衝，並製造出週期排列之金奈米結構。改變脈衝之振幅大小與時間長短，我們可以製造出坑與小山丘兩種結構。所製造之小山丘之金奈米結構，直徑約 10 奈米，高度為 1~2 奈米。

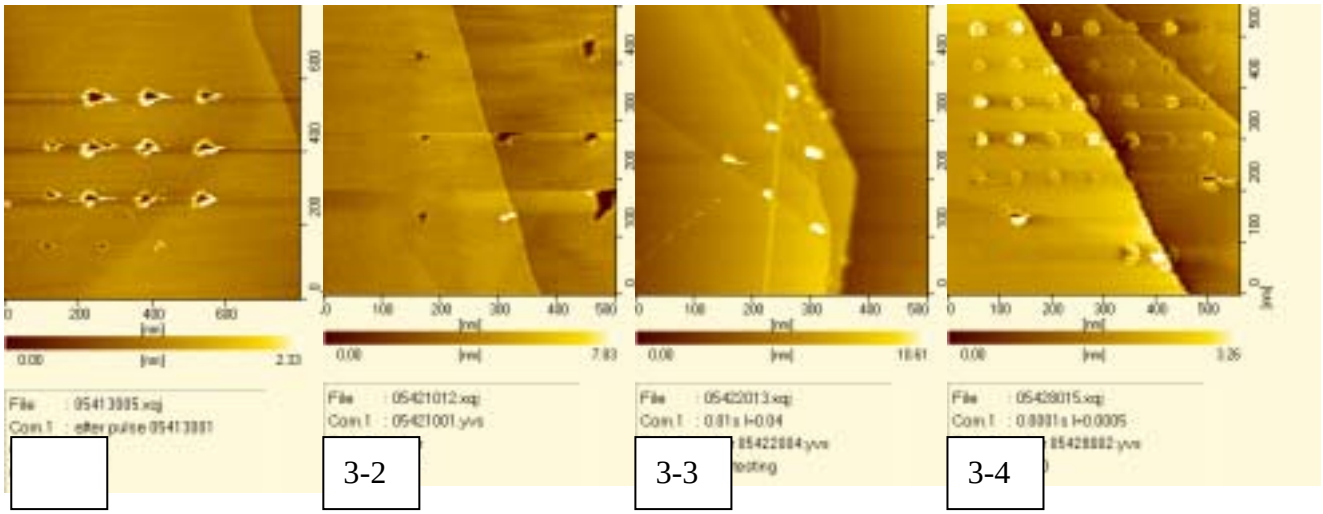

3-2 3-3 3-4

目前幾乎所有實驗都是在金塊材表面上使用金探針與脈衝高壓，製造坑洞與小山丘，我們選擇在石墨表面上，試圖製造奈米結構。圖 3-1 與 3-2 為石墨表面坑洞，製作方式為在不減小回饋線路反應情況下，在金探針與表面間外加一個 5 伏特 1 豪秒的脈衝，是由於金探針撞擊石墨所導致的坑洞。圖 3-3 仍舊不關閉回饋線路，此時延長脈衝時間達 10 豪秒，由於回饋線路啟動使得探針與樣品間的距離增加，又長時間的探針與樣品間處於高電壓能量的交互作用，導致表面產生金小山丘，此時的小山丘形貌較不規則，除了探針幾何形狀的因素外，長時間的交互作用易顯現出熱飄移與探針樣品間剛性問題。圖 3-4 為回饋線路反應最小時後，使用 5 伏特 0.1 豪秒製造之週期性排列金小山丘結構，當熱飄移問題較小時，在每次給電壓脈衝之前都在新的位置停留幾豪秒，等待探針與樣品之間恢復掃描時的距離才給脈衝，我們可製造出非常週期排列且大小相似的金奈米結構。

(4)奈米線電性研究

奈米線由下而上製造之電子元件將取代現有由上而下半導體製程製作之電子元件，因此了解奈米線之電性為重要課題。文獻上對 ZnO 奈米線兩點量測結果已經有許多報導，主要為將 ZnO 奈米線製作之裝置用來當光與氣體的微偵測器，而所報導之電流電壓曲線，可分為類似半導體 PN 結之結果，與類似 JFET 或 MOSFET 等電晶體之特性曲線兩種。由控制奈米線與金屬電極間奈米接點的絕緣層，我們可以由下而上做出這兩種不同裝置分別取代這些半導體元件。

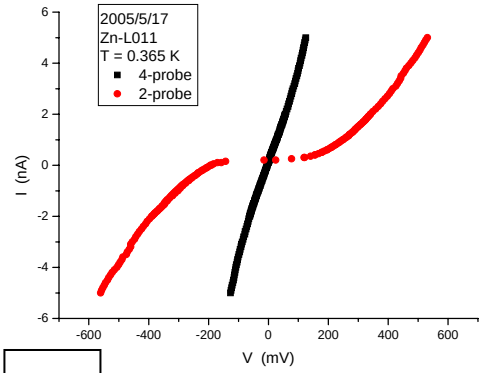

4-1

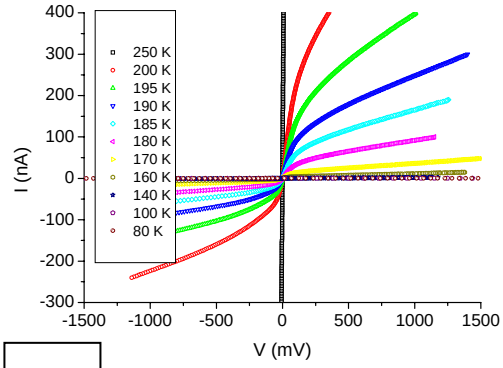

4-2

在對 ZnO 之電性有進一步了結之前，我們必須先對此金屬-半導體奈米接點之電流電壓特性曲線有所了解，正如控制半導體元件必須控制接面之表面效應一樣，我們必須對 ZnO 奈米線之表面與金屬電極之奈米接點有充分的研究。我們所量測到的電流電壓曲線，可分為來自兩個奈米接點，與來自 ZnO 奈米線，如圖 4-1 所示，因 ZnO 奈米線的電性接近歐姆定律，且貢獻很小，所以兩點量測 ZnO 奈米線之電流電壓特性，主要來自於奈米接點的貢獻。

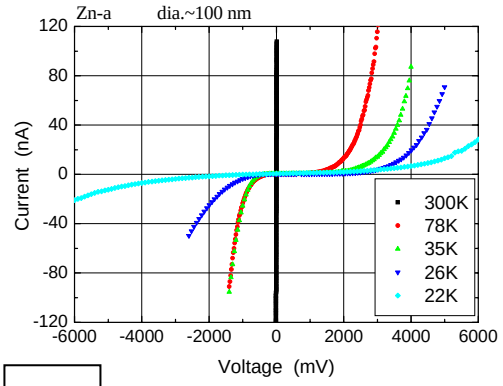

4-3

當此元件之室溫電阻小於 100 k 歐姆時，ZnO 奈米線與金屬電極間奈米接點電流電壓曲線，呈現飽和電流之曲線圖，如圖 4-2，且在同樣溫度與電壓下，其通過電流較大，此結果為穿隧電流的表現。當元件室溫電阻大於 100 k 歐姆，其電流電壓曲線轉為類似 PN 結之特性曲線，如圖 4-3，我們可以用兩個 PN 結來模擬實驗結果，與使用非線性偶合取得絕緣層穿隧位能障大小，此為熱電流的表現結果。

(5)自製掃描穿隧電流顯微鏡與小訊號測量儀器

製作掃描穿隧顯微鏡可分為機械設計、電子控制器與電腦介面及軟體等。

機械設計：包括外框架(outer frame)，內基台(inner stage)，彈簧懸吊系統，震盪阻泥系統，步進器，掃描器，探針與樣品座等方面。我們採用合金鋁在八吋 flange 上製作外框架，並使用兩層彈簧懸吊系統，與渦電流阻尼系統，採用垂直粘滑式步進器(約±20 V 即可驅動，克服重力)。

電子控制器與電腦介面：數位轉類比訊號 – 供給掃描器±x, ±y, z 軸與步進器所需之類比電壓。高電壓放大器 – 使用 TL783 製作直流高壓電源±125 V，使用 APEX PA15 運算放大器，將輸入之類比電壓轉成高壓輸入壓電材料。電流電壓轉換器 – 10^8 放大倍率，將電流轉成電壓訊號。回饋線路 – 電流轉電壓實際值與設定值之差值，加入 z 軸電壓。類比轉數位 – 取得實際 z 軸類比電壓轉換為數位，經由電腦介面讀入資料。

掃描探針顯微鏡之電子控制器，台製像中研院技術合作之冠球科技詢價約 100 萬，外購至少 160 萬。即使最簡單的提供掃描器±x, ±y, 與 z 軸放大的高壓輸出，也要 20 萬台幣，而我們已經製造出此電壓放大器。我們希望自製或找到具彈性的電子控制器，能很容易加入我們想要的新功能。

小訊號測量儀器

為了測量奈米線的電性，我們已製作出對稱式微小電流供應器，配合 Keithley 2000 我們可以測量奈米線的電阻與電流電壓曲線，在製作過程中，我們解決了小訊號量測所遭遇到的雜訊問題，並使用電池供應電源給運算放大器與良好的接地模式，去除 60 Hz 雜訊。在處理小訊號測量的過程中，我們學習到電源穩定性、電磁干擾防護與接地等知識，並因此成功解決前述之電流電壓轉換器雜訊問題。

Scanning Tunneling Microscope

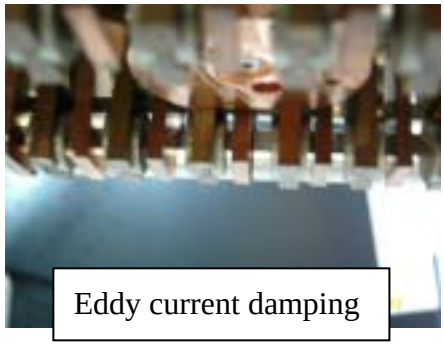

Eddy current damping

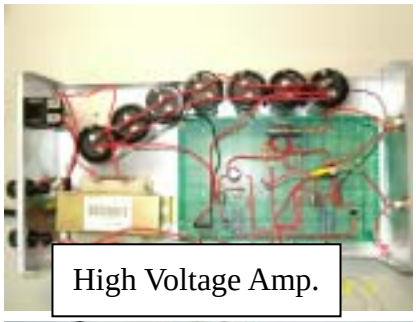

High Voltage Amp.

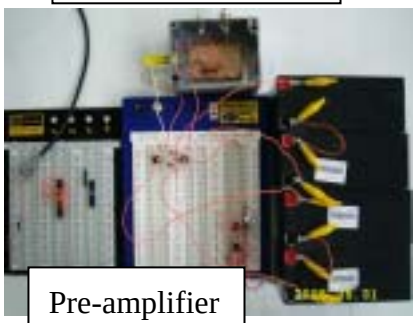

Pre-amplifier

參考文獻

計畫成果自評

因去年七月底自中興大學搬遷至交通大學電子物理系，交大新館實驗室空間今年初才啟用，計畫主持人認為還可以做得更好。感謝國科會的支持，讓本實驗室迅速發展起來。

Curie and Landau orbital susceptibilities of PbSe quantum dots

W. B. Jian,[1] Weigang Lu,[2] Jiye Fang,[2] S. J. Chiang,[3] M. D. Lan,[3] C. Y. Wu,[4] Z. Y. Wu,[5] F. R. Chen,[5] and J. J. Kai[5]

[1]*Department of Electrophysics, National Chiao Tung University, Hsinchu 300, Taiwan ROC*
[2]*Department of Chemistry and Advanced Materials Research Institute, University of New Orleans, New Orleans, Louisiana 70148*
[3]*Department of Physics, National Chung Hsing University, Taichung 402, Taiwan ROC*
[4]*Opto-Electronics and Systems Laboratories, Industrial Technology Research Institute, Hsinchu 310, Taiwan ROC*
[5]*Department of Engineering and System Science, National Tsing Hua University, Hsinchu 300, Taiwan ROC*

(Dated: May 27, 2005)

Different sizes of three dimensional PbSe quantum dots have been synthesized for the study of orbital magnetic susceptibilities. Two types of orbital susceptibilities have been found, including the Curie susceptibility and finite-size corrections to the Landau susceptibility. The Curie term of a quantum dot manifests itself in the temperature dependence of magnetic susceptibility at low temperatures while the field dependent differential susceptibility shows finite-size corrections to the Landau susceptibility. Both of the two orbital susceptibilities show linear dependence on the size. The experiments about finite-size corrections to the Landau susceptibility agree well with theoretical calculation of two dimensional quantum dots.

PACS numbers: 75.50.Tt, 75.75.+a, 73.21.La

Semiconductor and diluted magnetic semiconductor quantum dots (QDs) have drawn a lot of attention since their physical properties can be modified by the quantum confinement effects [1, 2, 3] and they possess a potential application in building spintronic devices such as quantum computer.[4] Recently, due to a successful development of synthetic methods, high quality preparation of many II-VI and IV-VI semiconductor QDs have been carried out and it has become possible to characterize their physical properties, especially the optical properties.[5, 6, 7, 8, 9]

Physics at mesoscopic scales often leads to striking phenomena due to intrinsic quantum effects.[10] Magnetic properties of materials, when transferred to the nano phase, may be much different from those in their bulk state. For example, carbon nanotubes, like two dimensional structures of graphite, exhibiting large diamagnetic susceptibility and owing mainly to orbital ring currents, have been studied experimentally and theoretically.[11, 12] Another example is that below a threshold diameter, Pd and Au nanoparticles, which correspond to para- and diamagnetic metal in bulk states, respectively, may display spontaneous magnetization.[13, 14, 15] According to a theoretical calculation, a mesoscopic tube is diamagnetic when the radius is larger than a threshold value, but becomes paramagnetic when its radius is smaller.[10]

Orbital magnetism had been an important theoretical work to understand the magnetic properties of ballistic billiard in mesocopic regime[16], for example, to explain the magnetization of a large amount of two dimensional semiconductor QDs which were fabricated by the lithography technique.[20] Two different theoretical approaches were adopted. One was taking quantum dots as atomiclike objects to demonstrate the orientational paramagnetism and precessional diamagnetism which were like the Curie and Langevin susceptibilities of atoms, respectively.[17] The oscillatory paramagnetic susceptibility as a function of the number of electrons in the QD were predicted. The other theoretical method was starting from the Landau susceptibility in bulk states. The free-electron diamagnetic susceptibility was then modified by finite-size corrections.[16, 18, 19] A zero-field paramagnetic peak which was firstly observed by Lévy et al.'s experiments[20] was reproduced theoretically. Recently, the experimental report[21] showed information about magnetization of two dimensional electron system and QDs which were differentiated in their field dependencies. The magnetization of QDs confirmed the zero-field paramagnetic peak.

Although quite a lot of theoretical works have been conducted to simulate the orbital magnetic response of QDs, the experimental studies of both the Curie and finite-size corrections to the Landau susceptibility of QDs have not been reported. With a help of high quality preparation of monodisperse semiconductor QDs[22, 23] and a careful separation of magnetic contribution from atoms and QDs, we report a direct observation of the two kinds of orbital magnetism.

7.9 g of selenium powder (99.999%, Aldrich) was added into 100 mL of TOP (trioctylphosphine, 90%, Aldrich) are stirred for overnight in a glove box to form a clear TOP-Se solution (1 M for Se). In a typical experiment, 1.081 g of lead acetate trihydrate [$(CH_3CO_2)_2Pb{\cdot}3H_2O$, 99.99+%, Aldrich, 2.85 m mol], 1.8 mL of oleic acid (90%, Aldrich) and 15 mL of phenyl ether were mixed and heated to 150 ^{o}C for 30 min under argon atmosphere. After the solution was cooled to 40 ^{o}C, it was transferred to a glove box and mixed with 4.0 mL of TOP-Se stock solution. This room-temperature mixed solution was then

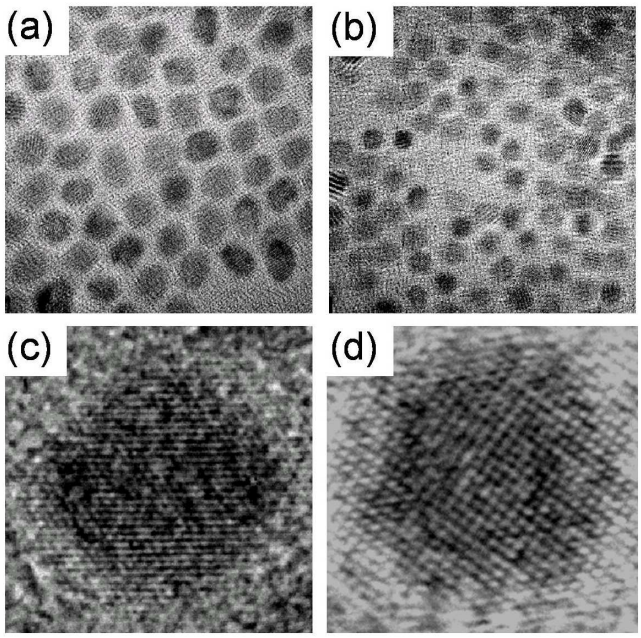

FIG. 1: TEM images of PbSe QDs with diameters of 10.5 nm ((a) and (c)), and 6.7 nm ((b) and (d)). The image sizes of (a) and (b) are 90 nm × 90 nm and the image sizes of (c) and (d) are 12.3 nm × 12.3 nm and 7.4 nm × 7.4 nm, respectively.

rapidly injected into vigorously stirred phenyl ether (15 mL) that was pre-heated to 150 ^{o}C in a three-neck flask equipped with a condenser under argon stream. After the injection, the temperature of the mixture dropped to about 135 ^{o}C and then was kept constant at 150 to 200 ^{o}C for 10 min, depending on the desired size of PbSe nanocrystals. The PbSe dispersion was then cooled and ethanol was added to flocculate the nanocrystals which were subsequently separated from solution by centrifugation. The size distribution of PbSe nanocrystals was further narrowed by a size-selection post-treatment using a pair of solvents, hexane/ethanol system.

PbSe QDs with different sizes have been prepared. The size distribution was monitored by using transmission electron microscope (TEM), where the standard deviation are 7.1% and 4.1% for QDs with diameters of 10.5 and 6.7 nm, respectively. The crystalline structure and the spherical shape of the PbSe QDs were confirmed by the high resolution TEM images shown in Fig. 1. The TEM images were carried out on a JEOL JEM-2010F. Magnetic properties of PbSe QDs were measured, over a temperature range of 2 to 300 K and a field from 0 to 50 kOe, by a SQUID magnetometer (Quantum Design MPMS-7). The magnetization of PbSe QDs is at least ten times larger than the sample holder background which is mainly from the capsule and is about -1×10^{-6} emu at 1 kOe. The susceptibility was calculated by dividing the molar grams of PbSe, not that of QDs.

The as-grown PbSe QDs stabilized with capping agents

TABLE I: Fitting results of 10.5-nm PbSe QDs

H (Oe)	χ_0 (emu/mol Oe)	C (emu K/mol Oe)	T_c (K)
1 k	2.7×10^{-4}	6.0×10^{-4}	-1.7
3 k	0.1×10^{-4}	6.9×10^{-4}	-1.5
5 k	-0.6×10^{-4}	5.6×10^{-4}	-1.4
10 k	-1.0×10^{-4}	6.1×10^{-4}	-1.9
30 k	-1.5×10^{-4}	7.4×10^{-4}	-8.6

TABLE II: Fitting results of 6.7-nm PbSe QDs

H (Oe)	χ_0 (emu/mol Oe)	C (emu K/mol Oe)	T_c (K)
3 k	2.6×10^{-4}	1.7×10^{-3}	-2.7
10 k	-1.9×10^{-4}	1.9×10^{-3}	-4.2
30 k	-3.3×10^{-4}	1.8×10^{-3}	-7.3

of both TOP and oleic acid. The total ratio of capping agents in all samples is ∼10 wt. % which was obtained by using differential scanning calorimetry and thermogravimetric analysis (DSC-TGA). The molecular susceptibilities from TOP and oleic acid are -3.20 and -2.10×10^{-4} emu/mol Oe, respectively.[24] The temperature and field independence of molecular susceptibilities of TOP and oleic acid, which are about -0.12 and -0.11×10^{-4} emu/mol Oe in our samples, were subtracted from the collected data. We also removed the contribution from the core diamagnetism of PbSe, taken as -1.0×10^{-4} emu/mol Oe in bulk states.[25] To examine the magnetization from contamination of magnetic impurities, a larger-size system of Mn-doped PbSe nanoarrays were synthesized.[23] We observed that the field dependence of magnetization of PbSe with Mn impurities had paramagnetic response under high magnetic fields while that of pure PbSe QDs didn't have any paramagnetic response at 5 K, even though the temperature dependence of molar susceptibilities and the Curie constants are the same. The following data is solely from the QDs.

How many electrons are there in a QD? If no free electron exists, we cannot observe any orbital susceptibility. A native hole-doping of PbSe is typically having a bulk carrier concentration of $\sim 10^{18}$ carriers/cm^3.[26] It generates less than one carrier per QD with a size of 10 nm. Besides doping carriers, it had been established that PbSe, when exposed to the air or oxygen, formed a strong p type surface layer and had high surface charge densities of 2-5×10^{13} carriers/cm^2.[26] We then estimate it being 15-40 carriers in the 10-nm sized QD when exposed to the air.

Temperature dependent susceptibilities are shown in Fig. 2. The magnetic susceptibilities of the PbSe QDs are given by $\chi = \chi_{C,atom} + \chi_{L,atom} + \chi_{C,QD} + \chi_{L,QD} + \chi_{Landau}$, where $\chi_{C,atom}$, $\chi_{L,atom}$, $\chi_{C,QD}$, and $\chi_{L,QD}$ are the atomic Curie, atomic Langevin, the QD's Curie,

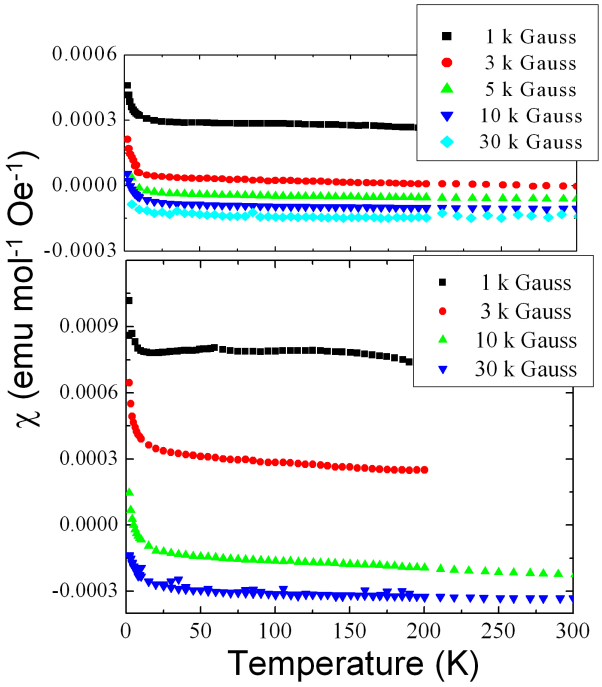

FIG. 2: Temperature dependence of susceptibilities of PbSe QDs under several external fields indicated in the graph. The susceptibilities are estimated per mole of PbSe.

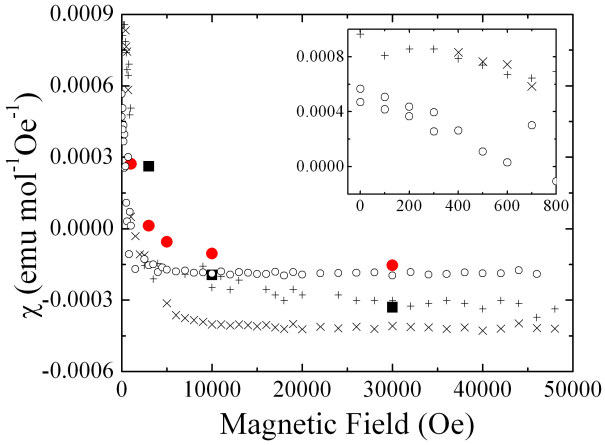

FIG. 3: Differential susceptibilities per mole PbSe. The open circles are calculated from field dependent magnetization of 10.5-nm QDs at 200 K. The crosses and the pluses represent susceptibilities of 6.7-nm QDs at 200 K and 5 K, respectively. The closed circles and squares are χ_0s in Table I and II of PbSe QDs with diameters of 10.5 and 6.7 nm, respectively. Inset: susceptibility in the low-field regime.

and the QD's Langevin susceptibilities, respectively, and χ_{Landau} is the contribution from finite-size corrections to the Landau susceptibility. The filled shells of electrons in PbSe result in a zero susceptibility of the atomic Curie term and the core Langevin diamagnetism is subtracted from data. The remaining contribution to the temperature dependent susceptibility is the Curie susceptibility of QDs. It can only be observed at temperatures $T < 10$ K and no field dependence of paramagnetism has been observed at a temperature exceeding 5 K. The disappearance of the QD's Curie susceptibility at a slightly higher temperature comes from the degraded quantization since the QDs have a much larger diameter compared to the size of atoms. The susceptibility as a function of temperature is fitted by $\chi = \chi_0 + C/(T - T_c)$, where χ_0 is a constant shift, C is the Curie constant, and T_c is the Curie or Weiss temperature. The samples studied under different external fields are listed in Table I and II. The fitted results show the same Curie constants for QDs with the same size and approve good fitting. The Curie constant of 6.7-nm QDs is ~ 2.8 times of that of 10.5-nm QDs. It roughly corresponds to $(10.5/6.7)^2$, that is proportional to D^{-2}, where D is the size of the QDs. An increase of Weiss temperature with a raising field may indicate a strong interaction in the QD. The positive shift of χ_0 is from the orbital Landau susceptibility, not from the Curie susceptibility.

A clear evidence of zero-field paramagnetic peak which agree well with the theory of finite-size corrections to the Landau susceptibility is shown in Fig. 3. The differential susceptibilities of both the 6.7- and 10.5-nm QDs taken at 200 K show paramagnetic with positive value under low fields and a transition to negatively saturated susceptibility under high magnetic fields. The saturated Landau diamagnetism in a high field gives -4.16 and -1.88×10^{-4} emu/mol Oe for 6.7- and 10.5-nm PbSe QDs, respectively. The orbital Landau susceptibility of the QDs per PbSe is several times larger than that of the atomic diamagnetism and varied with the diameter, D, as a function of D^{-2}. Differential susceptibilities under low magnetic fields is displayed in the inset of Fig. 3 to display its consistent enhancement in small-sized QDs. The temperature effect on the differential susceptibility is inspected for 6.7-nm QDs. It shows a broader zero-field paramagnetic peak at 5 K as comparing with data taken at 200 K. The constant shifts χ_0s listed in Table I and II are also plotted in Fig. 3. They tend to lie on the differential susceptibility taken at low temperatures.

For a flux quantum threading through a 10-nm QD, a magnetic field up to 130 kOe is needed. The extremely high field is required to see a complete cycle of oscillatory susceptibility. A transition from positive susceptibility to negatively saturated susceptibility in Fig 3 may be understood by using the magnetic length. If we consider it as a probing length of a QD, we need to apply a field higher than ~ 7.4 kOe to probe local magnetic properties of 10.5-nm QDs. The experimental result shows a transition field of ~ 3 kOe at 200 K. The same estimation gives

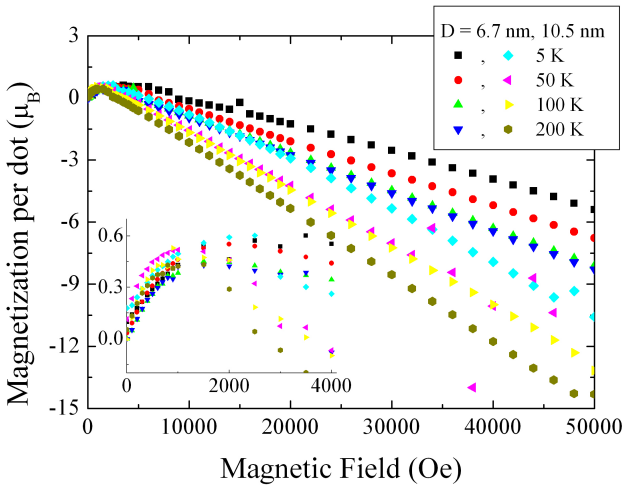

FIG. 4: Field dependence of magnetization per QD under high magnetic fields. Inset: magnetization under low magnetic fields.

a required field of $\sim$ 18.5 kOe for 6.7-nm QDs while our experiment shows $\sim$ 7 kOe at 200 K. The inconsistent transition fields between experiments and estimations result from the temperature effects.

We calculate the magnetization of a QD by multiplying the total number of PbSe unit cells and draw the field dependent magnetization in Fig. 4. It shows a small positive increase in a field lower than 1 kOe and a large decrease in a high field. The high-field magnetization exhibits linear dependence on magnetic fields at higher temperatures. Since the number of PbSe unit cells is proportional to D^3, and the Curie and finite-size corrections to the Landau susceptibilities per mole of PbSe are both proportional to D^{-2}, we find that the orbital magnetic susceptibilities of the QD vary linearly with its diameter as D^1. The results agree well with theoretical calculation of two dimensional QDs.[19] Here, we use the concept of thermal length $L_T = \hbar v_F/k_B T$ to see the temperature effect. A periodic orbit contributes significantly only if the size is of the order or shorter than the thermal length, $D < L_T$.[18] This leads to a relation $T < \hbar v_F/k_B D$. As the size of the QDs is smaller, the orbital susceptibility can be observed at a higher temperature. Comparing with previous experiments performed at 0.2 K and 8 K for QDs with sizes of 4.5 μm and 550 nm, respectively, the orbital susceptibility of the 10-nm QD can exist up to room temperature.

Two kinds of orbital susceptibilities, including the Curie and finite-size corrections to the Landau susceptibilities, have been observed in the three dimensional PbSe QDs. The temperature dependence of susceptibility at low temperature shows the Curie susceptibility of the QDs. In addition, the field dependence of differential susceptibility shows zero-field paramagnetic peak and reveals finite-size corrections to the Landau susceptibility. Both the two kinds of orbital susceptibilities display linear dependence on the size of the QD. Since the averaged susceptibility per PbSe unit cell decrease as a function of inverse square of the size, the susceptibilities from the QD disappears in the bulk state. Theories of orbital magnetization of two dimensional QDs adequately explain our experiments of three dimensional PbSe QDs.

This work was supported by the National Science Council of R.O.C. under Grant Nos. 93-2112-M-009-038. The author thank Dr. S. J. Cheng for helpful discussion.

[1] L. E. Brus, J. Chem. Phys. **80**, 4403 (1984).
[2] A. I. Ekimov, A. L. Efros, and A. A. Onushchenko, Solid State Commun. **56**, 921 (1985).
[3] A. P. Alivisatos, Science **271**, 933 (1996).
[4] S. A. Wolf, D. D. Awschalom, R. A. Buhrman, J. M. Daughton, S. von Molnar, M. L. Roukes, A. Y. Chtchelkanova, and D. M. Treger, Science **294**, 1488 (2001).
[5] R. N. Bhargava, D. Gallagher, X. Hong, and A. Nurmikko, Phys. Rev. Lett. **72**, 416 (1994).
[6] J. A. Gupta, D. D. Awschalom, X. Peng, and A. P. Alivisatos, Phys. Rev. B **59**, R10421 (1999).
[7] A. D. Andreev and A. A. Lipovskii, Phys. Rev. B **59**, 15402 (1999).
[8] F. R. Wise, Acc. Chem. Res. **33**, 773 (2000).
[9] H. Du, C. Chen, R. Krishnan, T. D. Krauss, J. M. Harbold, F. W. Wise, M. G. Thomas, and J. Silcox, Nano Lett. **2**, 1321 (2002).
[10] P. S. Davids, L. Wang, A. Saxena, and A. R. Bishop, Phys. Rev. B **48**, 17545 (1993).
[11] R. P. Ramirez, R. C. Haddon, O. Zhou, R. M. Fleming, J. Zhang, S. M. McClure, and R. E. Smalley, Science **265**, 84 (1994).
[12] J. P. Lu, Phys. Rev. Lett. **74**, 1123 (1995).
[13] H. Hori, T. Teranishi, Y. Nakae, Y. Seino, M. Miyake, and Y. Yamada, Phys. Lett. A **263**, 406 (1999).
[14] H. Hori, T. Teranishi, M. Taki, S. Yamada, M. Miyake, and Y. Yamamoto, J. Magn. Magn. Mater. **226-230**, 1910 (2001).
[15] H. Hori, Y. Yamamoto, T. Iwamoto, T. Miura, T. Teranishi, and M. Miyake, Phys. Rev. B **69**, 174411 (2004).
[16] K. Richter, D. Ullmo, and R. A. Jalabert, Phys. Rep. **276**, 1 (1996).
[17] Y. H. Zeng, B. Goodman, and R. A. Serota, Phys. Rev. B **47**, 15660 (1993).
[18] F. von Oppen, Phys. Rev. B **50**, 17151 (1994).
[19] D. Ullmo, K. Richter, and R. A. Jalabert, Phys. Rev. Lett. **74**, 383 (1995).
[20] L. P. Lévy, D. H. Reich, L. Pfeiffer, and K. West, Physica B **189**, 204 (1993).
[21] M. P. Schwarz, D. Grundler, M. Wilde, C. Heyn, and D. Heitmann, J. Appl. Phys. **91**, 6875 (2002).
[22] T. Ji, W.-B. Jian, and J. Fang, J. Am. Chem. Soc. **125**, 8448 (2003).
[23] W. Lu, P. Gao, W. B. Jian, Z. L. Wang, and J. Fang, J. Am. Chem. Soc. **126**, 14816 (2004).
[24] G. Föex, *Constantes Selectionnées Diamagnetisme et*

Paramagnetisme Relaxation Paramagnetique, vol. 7 (Masson, Paris, 1957).
[25] J. R. Anderson, G. Kido, Y. Nishina, M. Górska, L. Kowalczyk, and Z. Golacki, Phys. Rev. B **41**, 1014 (1990).
[26] M. H. Brodsky and J. N. Zemel, Phys. Rev. **155**, 780 (1967).

Annealing effects on ferromagnetic properties of Co-implanted ZnO nanowires

Z. Y. Wu, R. T. Huang, F. R. Chen, and J. J. Kai

Department of Engineering and System Science,

National Tsing Hua University, Hsinchu 300, Taiwan ROC

W. B. Jian

Department of Electrophysics, National Chiao Tung University, Hsinchu 300, Taiwan ROC

J. J. Lin

Department of Electrophysics and Institute of Physics,

National Chiao Tung University, Hsinchu 300, Taiwan ROC

Abstract

The $Zn_{1-x}Co_xO$ nanowires with an averaged diameter of ∼40 nm have been prepared by thermal evaporation method and then being ion implanted. The as-implanted nanowires were inspected in detail by X-ray diffraction, mapping of electron energy loss spectroscopy, and high resolution transmission electron microscope to make sure that no second phase exists down to a spacial limit of ∼1 nm. Two kinds of annealing processes, including annealing under an 1-atm argon flow and that in high vacuum at 600^oC, were performed and their effects on ferromagnetism in $Zn_{1-x}Co_xO$ nanowires were studied. The annealing in an argon flow at 1 atm recovers structural defects of stacking faults and orientation variations, and increases ferromagnetic order. The recovery of crystalline structure has been approved again in the analysis of electron energy loss spectra of Co element in $Zn_{1-x}Co_xO$ nanowires. The second kind of annealing process in high vacuum largely enhances ferromagnetism in $Zn_{1-x}Co_xO$ nanowires. It is suggested that the annealing in high vacuum not only removes structural defects but also increases oxygen vacancies as well as carrier concentration. Both the two kinds of annealing processes enhance ferromagnetic properties of Co-implanted ZnO nanowires.

Structure effects on ferromagnetism in $Zn_{1-x}Co_xO$ nanowires

W. B. Jian*
Department of Electrophysics, National Chiao Tung University, Hsinchu 300, Taiwan, ROC

Z. Y. Wu, R. T. Huang, F. R. Chen, and J. J. Kai
Department of Engineering and System Science, National Tsing Hua University, Hsinchu 300, Taiwan, ROC

C. Y. Wu
Opto-Electronics and Systems Laboratories, Industrial Technology Research Institute, Hsinchu 310, Taiwan, ROC

S. J. Chiang and M. D. Lan
Department of Physics, National Chung Hsing University, Taichung 402, Taiwan ROC

J. J. Lin*
Department of Electrophysics and Institute of Physics, National Chiao Tung University, Hsinchu 300, Taiwan, ROC

Diameter controllable crystalline ZnO nanowires, with the [0001] growth direction in the plane, have been fabricated by using the thermal evaporation method. The as-grown nanowires with diameter of $\sim$ 40 nm were implanted with various amounts of Co ions. The as-implanted $Zn_{1-x}Co_xO$ ($x \leq 0.11$) nanowires exhibited paramagnetic, but not ferromagnetic, behavior, and possessed high density of radiation induced orientation variations and stacking faults. After annealing the structural defects largely disappeared, and noticeable hysteresis in the magnetization loops revealed apparent ferromagnetic ordering in the nanowires. This work supports the idea of carrier-mediated ferromagnetism in diluted magnetic semiconductors having a long transport mean free path.

Not only high Curie temperature but also the mechanism of carrier-induced ferromagnetism in diluted magnetic semiconductors (DMS) has recently drawn much experimental and theoretical attention. It has been proposed that the ferromagnetism in III-V based DMS materials, (In,Mn)As and (Ga,Mn)As, is mediated by the mobile holes originating from the magnetic Mn-dopants[1–3]. The ferromagnetic p-type (Ga,Mn)As with a high carrier density (10^{18}–10^{20} cm^{-3}) could possess Curie temperature as high as 110 K.[3] It has also been argued that the Curie temperature of the p-type Mn-doped ZnO semiconductor, with a carrier concentration of 3.5×10^{20} cm^{-3}, could be as high as the room temperature. Recently, these theoretical proposals have stimulated numerous experimental works in an effort to search for high Curie temperature DMS ferromagnets.[4–6] In particular, *ab initio* theoretical calculations predicted a stable ferromagnetic phase in the n-type ZnO with Co doping.[7, 8] Experimentally, significant discrepancies have been reported among different groups and between the measurements and theoretical calculations. The widely proposed mechanism of carrier-induced ferromagnetism in Co-doped ZnO nanowires has not been clarified in the experiment.

ZnO is an oxide semiconductor with a room temperature energy gap of 3.37 eV. In contrast to the other II-VI compound semiconductors, ZnO can be heavily doped with electrons to form a transparent conductor. Since nanostructures are potentially ideal functional components in the future nanometer-scale electronics and optoelectronics, the study of ZnO nanowires is currently of high interest. Realization of spintronic devices from the bottom up would be feasible by adopting the DMS Co-doped ZnO nanowires.[9, 10]

In addition to the carrier concentration, it is theoretically accepted that crystalline quality and structural defects should play an important role in the occurrence and stability of ferromagnetism.[11–13] Thus far, there has been no clear experimental observation to discern this conjecture. In this work, we use natively doped crystalline n-type[14] ZnO nanowires, implanted with Co ions, to investigate the correlations between the structural defects and the strength of ferromagnetism.

ZnO powder was placed in a crucible situated at the center of a quartz tube in a furnace heated to 950°C. A glass substrate at a temperature of 500°C with gold nanoparticles ($\sim$ 40 nm in diameter) as catalysts predeposited on it was located at the downstream end of the quartz tube. The chamber was maintained at 200 Pa with a constant flow of argon. After 8 hours, ZnO nanowires with an average diameter of 40 nm was formed on the glass substrate. The as-grown ZnO nanowires were implanted by Co ions with doses of $(1–6)\times10^{16}$ cm^{-2}. The implantation was performed at room temperature with an accelerating energy of 40 keV by using

*Authors to whom correspondence should be addressed; electronic mail: wbjian@mail.nctu.edu.tw; jjlin@mail.nctu.edu.tw

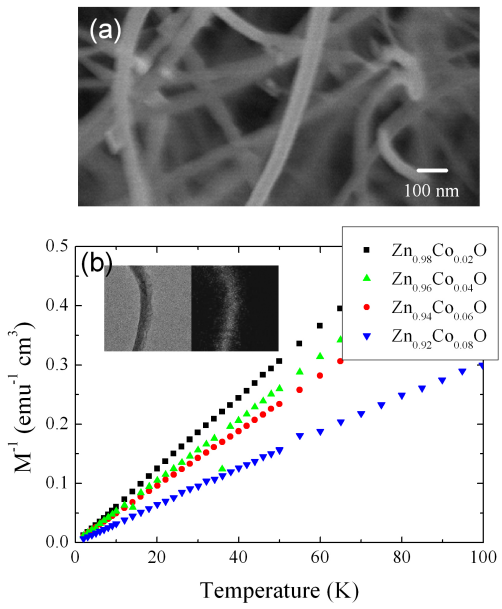

FIG. 1: (a) A typical SEM image of the as-implanted $Zn_{0.94}Co_{0.06}O$ nanowires. (b) The inverse magnetizations of $Zn_{1-x}Co_xO$ nanowires taken at a field of 1000 Oe. The nanowires reveal paramagnetic behavior, and the paramagnetism enhances with increasing Co doping. Insets: An TEM image of a nanowire (left) together with its corresponding EDX mapping image (right) shows an uniform distribution of Co ions in the nanowires.

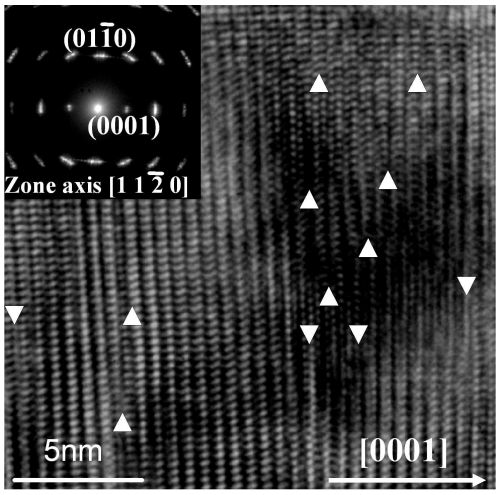

FIG. 2: An HRTEM image of as-implanted $Zn_{0.89}Co_{0.11}O$ nanowires with white triangles indicating stacking faults. Inset: A typical diffraction pattern revealing a rotation of reciprocal lattice points.

a tandem accelerator (9SDH-2). The beam current was kept at 150 nA/cm^2 to avoid beam heating. Annealing of the as-implanted ZnO nanowires was then performed at 600°C in a tube furnace under an argon flow of 150 sccm at 1 atm for 12 hours. This annealing temperature would not cause segregation and clustering of the implant ions, as was established previously for ZnO[15] and was confirmed by our HRTEM studies. The annealing at 1 atm prevented any significant change in carrier concentration.[13, 16, 17] Both the as-implanted and annealed ZnO nanowires were characterized by using field-emission scanning electron microscope (JEOL JSM-6330F) and high-resolution transmission electron microscope (JEOL JEM-2010F). Magnetic properties of the nanowires were studied by using a Quantum Design SQUID magnetometer. All the magnetizations as a function of applied field were taken at 2 K.

Most of the ZnO nanowires lay on the substrate with [0001] growth direction in the plane. The high energy Co ions were bombarded on one side of the ZnO nanowires to form DMS nanowires. Computer simulation SRIM code[18] enabled us to estimate the distribution of Co ions in the ZnO nanowires. The Co-ion density distribution as a function of penetration depth showed a peak at 20 nm. The SRIM simulation predicted a range of Co ions about the diameter ($\sim$ 40 nm) of our nanowires.

Figure 1(a) shows an SEM image of representative as-implanted nanowires. We found that the morphology and dimension of the ZnO nanowires did not change appreciably after implantation, except some slight bending of the nanowires. The energy dispersive X-ray spectroscopy (EDX) compositional map shows Co distribution in the right image of the inset in Fig. 1(b), in comparison to the bright field TEM image in the left. The estimated thickness of a layer of DMS nanowires on the substrate was about 110 nm which was $\sim$ 2 times larger than the estimated ion range by using SRIM code simulation. Figure 1(b) shows a plot of the inverse magnetizations of our $Zn_{1-x}Co_xO$ nanowires with several concentrations x as indicated. These as-implanted nanowires display paramagnetism closely obeying the Curie law. As x increases, the paramagnetism is enhanced, being in accord with the Co concentrations determined from the EDX spectra.

The as-implanted nanowires exhibit paramagnetism, whereas they vaguely reveal ferromagnetic ordering (see squares in Fig. 3(a)). The structural defects produced during the high energy Co-ion bombardment were expected and inspected in detail. The HRTEM image shown in Fig. 2 displays one type of structural defects, i.e., stacking faults, as indicated by the many small triangles. Another type of structural defects is orientation variations. The inset of Fig. 2 shows a typical diffraction pattern of which for the representative as-implanted $Zn_{0.89}Co_{0.11}O$ nanowires. One sees that the lattice planes along the [0001] direction are fairly ordered while there is orientation variation between the $(11\bar{2}0)$ lattice planes. The latter leads to appreciable disorder in the other directions.

Thermal annealing was performed on our nanowires and magnetizations were then remeasured. Figure 3(a)

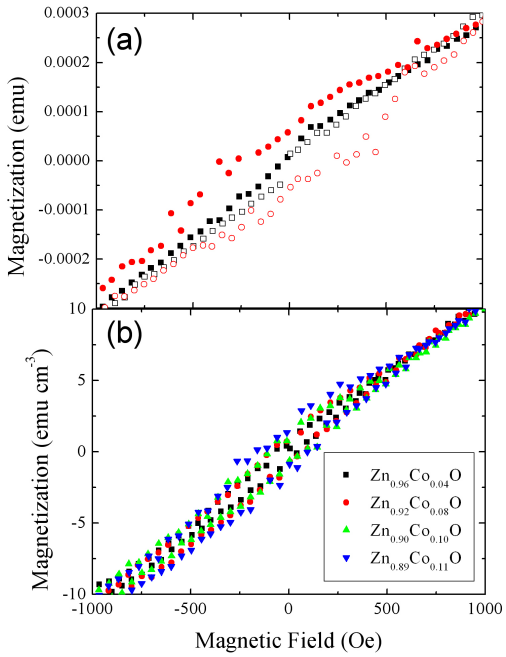

FIG. 3: (a) Magnetization as a function of applied field at 2 K, squares and circles represent as-implanted and annealed $Zn_{0.89}Co_{0.11}O$ nanowires, respectively. (b) Magnetization as a function of applied field at 2 K for annealed $Zn_{1-x}Co_xO$ nanowires with different Co concentrations as indicated. The magnetization for each concentration has been scaled by dividing the factor of its concentration.

shows the field dependent magnetizations of the representative $Zn_{0.89}Co_{0.11}O$ nanowires. The open and closed circles, respectively, stand for the forward and backward sweeping of the magnetic field. For all Co concentrations, the as-implanted nanowires revealed negligible hysteresis while the annealed nanowires displayed distinct ferromagnetism as evidenced in the hysteresis loop (circles in Fig. 3(a)). This comparison study of the as-implanted and annealed samples enable us to identify the mechanism for the enhanced ferromagnetism, i.e., structural defects are detrimental to the occurrence of ferromagnetic ordering. Figure 3(b) shows the magnetizations of $Zn_{0.96}Co_{0.04}O$, $Zn_{0.92}Co_{0.08}O$, $Zn_{0.90}Co_{0.10}O$, and $Zn_{0.89}Co_{0.11}O$ nanowires divided by a factor of 4, 8, 10, and 11, respectively, for comparison. One sees that the hysteresis loops become more profound with increasing Co concentration, implying the formation of domains as well as the enhanced exchange interactions between Co ions. Meanwhile, the magnetization increases with increasing Co-ion implantation, confirming the existence of ferromagnetic, but not previously reported antiferromagnetic[12], order among Co ions.

The structure of the annealed $Zn_{1-x}Co_xO$ nanowires was then inspected by HRTEM. The diffraction pattern

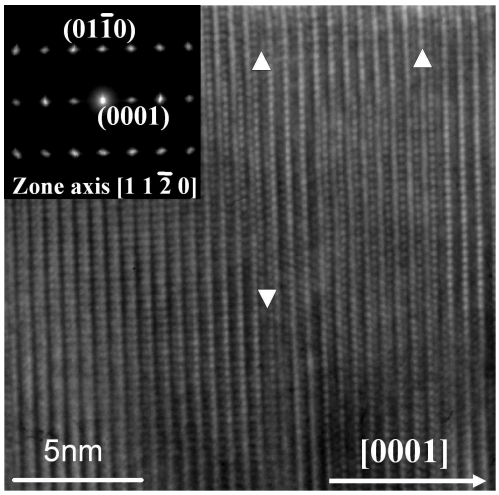

FIG. 4: An HRTEM image of annealed $Zn_{0.89}Co_{0.11}O$ nanowires with white triangles indicating stacking faults. Inset: A typical diffraction pattern showing regular reciprocal lattice points.

in the inset of Fig. 4 clearly shows disappearance of orientation variations. The lattice points along the $[01\bar{1}0]$ direction are now well ordered. Moreover, the HRTEM image of the annealed $Zn_{0.89}Co_{0.11}O$ in Fig. 4 shows a significant reduction in the density of stacking faults. Therefore, it is clear that the improved lattice order in the annealed DMS Co-ZnO nanowires leads to enhanced ferromagnetism. Before annealing, ferromagnetic ordering was deprived due to the presence of a high density of orientation variations and stacking faults. This result strongly suggests that the electron transport with a long mean free path is crucial to the carrier-induced ferromagnetism in Co-ZnO nanowires.

To summarize, 40-nm diameter $Zn_{1-x}Co_xO$ ($x \leq 0.11$) nanowires were synthesized by thermal evaporation, followed by high energy Co-ion implantation. The implanted Co ions were uniformly distributed in the nanowires and they produced many orientation variations and stacking faults as structural defects. After annealing the crystalline lattice order was essentially recovered. The magnetizations then indicated apparent ferromagnetic behavior. This observation is strongly supportive of the current idea of the carrier-mediated ferromagnetism in DMS $Zn_{1-x}Co_xO$ nanowires.

This work was supported by the National Science Council of R.O.C. under Grant Nos. 93-2112-M-009-038 and 93-2120-M-009-009.

[1] T. Dietl, H. Ohno, F. Matsukura, J. Cibert, and D. Ferrand, Science **287**, 1019 (2000).
[2] H. Akai, Phys. Rev. Lett. **81**, 3002 (1998).
[3] F. Matsukura, H. Ohno, A. Shen, and Y. Sugawara,

Phys. Rev. B **57**, R2037 (1998).
[4] K. Ueda, H. Tabata, and T. Kawai, Appl. Phys. Lett. **79**, 988 (2001).
[5] H.-J. Lee, S.-Y. Jeong, C. R. Cho, and C. H. Park, Appl. Phys. Lett. **81**, 4020 (2002).
[6] D. P. Norton, S. J. Pearton, A. F. Hebard, N. Theodoropoulou, L. A. Boatner, and R. G. Wilson, Appl. Phys. Lett. **82**, 239 (2003).
[7] K. Sato and H. Katayama-Yoshida, Jpn. J. Appl. Phys., Part 2 **40**, L334 (2001).
[8] N. A. Spaldin, Phys. Rev. B **69**, 125201 (2004).
[9] Y. Ohno, D. K. Young, B. Beschoten, F. Matsukura, H. Ohno, and D. D. Awschalom, Nature **402**, 790 (1999).
[10] S. A. Wolf, D. D. Awshcalom, R. A. Buhrman, J. M. Daughton, S. von Molnár, M. L. Roukes, A. Y. Chtchelkanova, and D. M. Treger, Science **294**, 1488 (2001).
[11] Y. W. Heo, M. P. Ivill, K. Ip, D. P. Norton, S. J. Pearton, J. G. Kelly, R. Rairigh, A. F. Hebard, and T. Steiner, Appl. Phys. Lett. **84**, 2292 (2004).
[12] A. S. Risbud, N. A. Spaldin, Z. Q. Chen, S. Stemmer, and R. Seshadri, Phys. Rev. B **68**, 205202 (2003).
[13] Y. M. Cho, W. K. Choo, H. Kim, D. Kim, and Y. Ihm, Appl. Phys. Lett. **80**, 3358 (2002).
[14] F. Tuomisto, V. Ranki, K. Saarinen, and D. C. Look, Phys. Rev. Lett. **91**, 205502 (2003).
[15] E. Sonder, R. A. Zuhr, and R. E. Valiga, J. Appl. Phys. **64**, 1140 (1988).
[16] A. Tiwari, C. Jin, J. Narayan, and M. Park, J. Appl. Phys. **96**, 3827 (2004).
[17] C. Ronning, P. X. Gao, Y. Ding, Z. L. Wang, and D. Schwen, Appl. Phys. Lett. **84**, 783 (2004).
[18] J. F. Ziegler and J. P. Biersak, http://www.srim.org.